Structural Effects in the Protonic/Electronic Conductivity of Dion-Jacobson Phase Niobate and Tantalate Layered Perovskites

Yoji Kobayashi,[†] Joshua A. Schottenfeld,[†] Digby D. Macdonald,[‡] and Thomas E. Mallouk*,[†]

Department of Chemistry, 104 Chemistry Building, The Pennsylvania State University, University Park, Pennsylvania 16802, and Center for Electrochemical Science and Technology, Department of Materials Science and Engineering, The Pennsylvania State University, University Park, Pennsylvania 16802

Received: May 18, 2006; In Final Form: October 15, 2006

The layered Dion-Jacobson phase perovskites $HLaTa_2O_7 \cdot xH_2O$, $HLaNb_2O_7 \cdot 0.5H_2O$ and structural variants of $HLaNb_2O_7 \cdot 0.5H_2O$ were prepared and their AC and DC conductivities were measured as a function of temperature and atmosphere. The layered structure in $HLaNb_2O_7 \cdot 0.5H_2O$ was modified by pillaring, exfoliation-restacking, and further annealing. Exfoliation followed by restacking markedly increased the ionic conductivity, either by creation of mesopores for hydration or by enhanced contact between layers, but pillaring had little effect. $HLaNb_2O_7 \cdot 0.5H_2O$ was prone to reduction under hydrogen, yielding a mixed ionic-electronic conductor. In-plane conductivity measurements of an oriented film of $HLaNb_2O_7 \cdot 0.5H_2O$ showed enhanced ionic conductivity attributed to the anisotropic conductivity of the sheets, but reduction under a hydrogen atmosphere was apparent. The reduction could be suppressed by adding water vapor to the ambient atmosphere or by replacing the B-site niobium with tantalum, which is less easily reduced.

Introduction

Currently, much research on fuel cells focuses on low-temperature polymer electrolyte fuel cells (PEMFC) and high temperature solid oxide fuel cells (SOFC). PEMFC and SOFC technologies are both promising because good proton and oxide ion conductor materials are available for the appropriate temperature ranges. In the intermediate temperature range (250−400 °C), however, there are few thermally stable materials that have the high ionic conductivity (10^{-1} to 10^{-3} S/cm) needed for fuel cell membranes.[1] Compared to PEMFCs, fuel cells operating in the intermediate temperature regime are more resistant to catalyst poisoning by CO, and a wider range of less expensive catalysts can be used. Because of their lower operating temperature, intermediate temperature fuel cells are less affected by the materials engineering issues stemming from the high temperatures used in SOFCs.

The polymeric membranes used in PEMFCs lose conductivity above 100 °C because of dehydration, and most ion conducting polymers are chemically unstable in the intermediate temperature regime. A number of polymer−inorganic composites and polymers combined with nonaqueous liquid proton conductors have been studied for use between 100 and 200 °C.[2] Recently, poly(benzoimidazole) derivatives, such as poly[2,5-benzimidazole], have been reported to be stable up to 200 °C.[3] However, even these suffer from loss of the dopant, phosphoric acid, at higher temperatures.

On the other hand, a number of inorganic solids such as $BaCeO_3$,[4] $Ba_3Ca_{1.18}Nb_{1.82}O_{9-\delta}$ (BCN18),[5,6] and CsH_2PO_4[7] are known to have appreciable proton conductivity at temperatures between 250 and 600 °C.[4,6] Layered solid acids such as α-$Zr(HPO_4)_2 \cdot H_2O$,[8] which retain intercalated water molecules, can have appreciable protonic conductivity at even lower temperatures. In these materials, the layers act as conduction channels for protons and water. The disadvantages of layered solid acids include irreversible dehydration at temperatures from 300 to 400 °C. These issues are sometimes a hindrance not only in operation, but also in processing or fabrication of membrane-electrode assemblies, since high-temperature steps such as sintering cannot be performed.

Layered inorganic solids undergo exfoliation, restacking, and pillaring reactions that can in principle be useful in fabricating intermediate temperature membranes and membrane−electrode assemblies. The Dion−Jacobson phase layered perovskite $HLaNb_2O_7$ has already been modified by all of these processes.[9−12] Furthermore, this compound has been shown to be quite acidic and to retain mobile lattice protons up to 400 °C under dry atmospheres.[13] Although no general thermodynamic data exist, these types of acidic perovskites are thought to be metastable compounds, and the dehydration of $HLaNb_2O_7$ to $LaNb_2O_{6.5}$ is irreversible. Previous studies have shown that several layered perovskites, including $HLaNb_2O_7$, exhibit ionic conductivities of 10^{-5}−10^{-3} S/cm at temperatures between 300 and 600 °C.[14−16] Sato et al. reported that for $HLaNb_2O_7 \cdot 0.5H_2O$ the adsorbed water, rather than interlayer protons, were the dominant cause of proton conductivity at temperatures below 80 °C, but they did not investigate the conductivity of the compound in the intermediate temperature regime.[17] In this study, the structure of the layered perovskite $HLaNb_2O_7 \cdot 0.5H_2O$ was modified in various ways to increase the surface area for water adsorption and to optimize the conduction paths. The effect of reducing conditions, such as the presence of hydrogen at elevated temperatures, was investigated, and methods to suppress the electronic conductivity caused by reduction were also explored.

Experimental Section

Sample Synthesis. Starting materials $RbLaNb_2O_7$, and their tantalate analogues, were prepared by reaction of Nb_2O_5, Ta_2O_5,

* To whom correspondence should be addressed. E-mail: tom@chem.psu.edu.
[†] Department of Chemistry.
[‡] Department of Materials Science and Engineering.

10.1021/jp063061d CCC: $37.00
Published on Web 01/27/2007

and Rb_2CO_3 (20% excess) at 1150 °C for 2 days. The phase purity of $RbLaNb_2O_7$ was confirmed by powder X-ray diffraction. The resulting alkali compounds (1 g) were then acid exchanged by shaking in 100 mL of 4 M HNO_3 for at least 3 days with daily centrifugation and replacement of the acid solution. The product was isolated by centrifugation, washing, and finally drying at 60 °C. However, if the next intended step was exfoliation, then the sample was not dried and instead was kept as a slurry in water.

Exfoliation/Flocculated Samples. For exfoliation, a larger batch of the protonated compound (4 g, 9.1 mmol) was shaken at 200 rpm for at least 2 days with 8.5 equiv (3.6 wt %, 550 mL) of aqueous tetra(*n*-butyl)ammonium hydroxide (TBAOH). The flocculated samples were prepared by taking 300 mL of the suspension, removing excess TBAOH by centrifugation, and then adding HNO_3 (1L, 0.05 M) dropwise overnight.

Silica-Pillared Sample. A literature procedure based on Guo et al. was adapted.[9] A hexylamine solution of ethanol (50% vol, 12 mL) was added to $HLaNb_2O_7$ (1 g), and stirred at 60 °C for 4 days to obtain an intercalated product (d = 24.2 Å). The suspension was washed with ethanol, and a decylamine solution of ethanol (50% vol, 12 mL) was added and refluxed for two weeks. This decylamine intercalated material (d = 29.4 Å) was then washed with ethanol and further refluxed with either an ethanol solution or a water sol of 3-aminopropyltriethoxysilane (25% vol, 50 mL) for 4 days before washing with ethanol. The siloxane-oligomer intercalated material was then calcined at 500 °C overnight to obtain the final pillared product. TGA-MS verified the release of CO_2 and NO_2 slightly below this temperature.

Thin-Film Preparation. For thin film preparation, the colloidal suspensions of exfoliated materials (50 mL) were centrifuged, decanted, and then resuspended in ethanol (5 mL) by agitation, and then cast onto glass slides patterned with Pt electrodes. Typically, 5−6 drops were applied to a glass square (2 cm × 2 cm) with intermittent drying. The Pt patterns consisted of a gap 800 μm wide and 1.5 cm long (conduction in the 800 μm direction) between Cr/Pt pads (150 nm thick) prepared by lithography and sputtering techniques. Removal of organics from the thin films was accomplished by heat treatment at 350 °C or by exposure to UV−O_3 (either at room temperature or 80 °C) until X-ray diffraction showed a single and constant *d*-spacing 00l reflection.

Impedance Measurements. Pellet samples were prepared by pressing 0.5 g of material at 220 MPa for 20 min. Unless otherwise noted, pellets (13 mm in diameter, and approximately 1 mm thick) were coated on both sides with 150 nm of Pt by sputtering to produce circular contacts 9 mm in diameter. Room temperature measurements were obtained by equilibrating the pellets under a stream of humidified air (100%RH, room temperature) overnight. Elevated temperature experiments were conducted using a home-built flow-through system with a H_2 stream of 30 mL/min humidified at P_{H_2O} = 0.3 atm. Two point impedance measurements were obtained using a Solartron 1255B Frequency Response Analyzer and Solartron 1287 Electrochemical Interface with no DC bias and an alternating voltage amplitude ranging between 50 to 500 mV. Frequencies ranged from 1 MHz to 0.01 Hz, depending on the sample. Kramers−Kronig transforms were conducted on select data to test the data for conformity to the stability, causality, and linearity constraints of linear systems theory. Previous work on electrochemical systems has shown that Kramers−Kronig transforms are most sensitive to violation of the stability constraint[18] and thus provide a means to verify if the sample was stable and at equilibrium during measurement. Further details on the transforms are included in the Supporting Information section.

DC Conductivity Measurements. Pellets with Toray carbon paper backings on both sides were pressed at the same conditions as above. The porous carbon paper was used as an electrode instead of platinum films to ensure fast responses of the pelletized material to the hydration environment. Leads were then applied using silver paint, and the pellets were treated under various gases and humidities in an in-house constructed flow-through system.

Other Characterization. X-ray powder diffraction patterns were obtained on a Philips XPert system using Cu Kα radiation. Brunauer−Emmett−Teller (BET) surface areas and N_2 adsorption isotherms were acquired at 77 K using a Micromeritics 2010 ASAP system. A Nanoscope atomic force microscope (AFM) and NPX200 SII profilometer were used to observe exfoliated material and deposited films. Electron micrographs were obtained using a FEI Quanta 200 scanning electron microscope (SEM) equipped with energy dispersive X-ray spectroscopy (EDS). Thermal gravimetry-mass spectrometry (TGA-MS) was conducted on a TA instruments Q50 thermal gravimetric balance (1 °C/min) in tandem with a Pfeiffer quadrupole mass spectrometer.

Results and Discussion

X-ray diffraction (XRD) patterns of the parent material $HLaNb_2O_7$ and its tantalum analogues were in good agreement with the literature.[19] Samples of $HLaNb_2O_7$ and $HLaTa_2O_7$ were equilibrated overnight at ambient temperature and at 100% relative humidity; water loss upon subsequent heating was then quantified by thermal gravimetry analysis (TGA). (See the Supporting Information for additional XRD and TGA data.) Sato et al. have shown that when $HLaNb_2O_7$ is equilibrated under 100% relative humidity at ambient temperature it hydrates to $HLaNb_2O_7{\cdot}0.5H_2O$ with a *c* lattice parameter of 11.404 Å, whereas the anhydrous material has a *c* lattice parameter of 10.548 Å.[17] Based on XRD and TGA, our own samples were anhydrous in ambient atmosphere and hydrated to a lower level of $HLaNb_2O_7{\cdot}0.25H_2O$ at 100% RH. However, Sato's formulation of $HLaNb_2O_7{\cdot}0.5H_2O$ will be used for naming the hydrated compound in this paper, since it is possible that water was lost during sample transfer. It is also possible that the dehydration behavior depends on other factors in sample preparation, since Sato et al. note that water is gradually lost between 100 and 400 °C (no heating rate given)[17] whereas Matsuda et al. see little loss between 100 and 400 °C (10 °C/min).[13] Our own TGA results show that for the niobate and tantalate water adsorbed at 100% RH at ambient temperature is lost upon exposure to dry air rather quickly below 100 °C, and there is very little further weight loss over the range 100−400 °C. An abrupt weight loss at 400 °C for $HLaNb_2O_7$ corresponds to irreversible dehydration to $LaNb_2O_{6.5}$, releasing 0.5 mol H_2O per mol of $HLaNb_2O_7$. This dehydration temperature is close to that reported previously.[13]

Impedance spectra of both materials are shown in Figure 1, and the intercept on the real axis (approximately 260 kΩ·cm here but ranging up to 600 kΩ·cm, depending on the sample) for $HLaNb_2O_7{\cdot}0.5H_2O$ corresponds reasonably well with that reported by Sato et al. (approximately 400 kΩ·cm).[17] Sato et al. conducted their lowest frequency measurements at 40 Hz, and since they observed only one semicircle, they proposed that they could not resolve grain boundary and grain bulk components. When measurements are extended to 0.01 Hz as shown

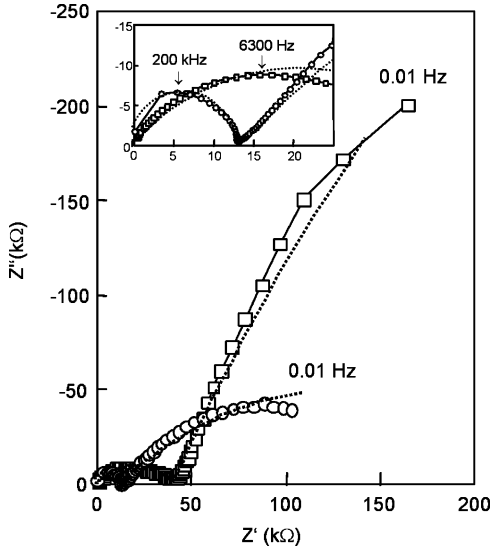

Figure 1. Impedance spectra (1 MHz ~ 0.01 MHz) at room temperature, under wet air ($P_{H_2O} = 0.03$ atm). Dotted lines are fits to models shown in Figure 2. □: $HLaNb_2O_7 \cdot 0.5H_2O$, ○: $HLaTa_2O_7 \cdot 0.5H_2O$ (pellet with half the area).

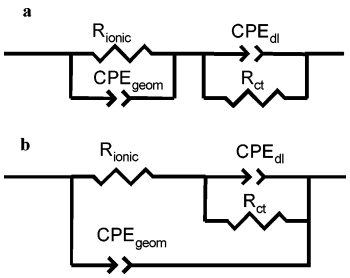

Figure 2. Equivalent circuit models.

in Figure 1**,** the tail starts to curve into another semicircle, notably in the tantalum case. We postulate that the relaxation at high frequency is due to the grain surface conductivity whereas that at lower frequency is due to electrode polarization. Although higher temperature proton conductors, such as BCN18, have been reported to have quite low grain boundary conductivities,[20] our materials differ from these because in layered perovskites the conductivity does not originate from hydrated oxygen vacancies in the lattice; rather, conductivity originates from water adsorbed on surfaces. Grain bulk conductivity from interlayer hydrated protons in $HLaNb_2O_7$ is probably insignificant because the overall conductivity measured in air drastically decreased when the temperature was raised from ambient temperature to 110 °C, despite the higher absolute humidity ($P_{H_2O} = 0.3$ atm as opposed to 0.03 atm). This agrees with results by Sato et al., who found that the conductivity is related to water content and follows a Freundlich-type isotherm, $\sigma \propto P_{H_2O}^{1/n}$, where $1/n$ expresses the density of water adsorption on a rough surface.[17]

An equivalent circuit shown in Figure 2 fits the spectra of the niobate and tantalate reasonably well, as shown by the dotted lines in Figure 1. Since the semicircle features were depressed, constant phase elements (CPE) were used instead of capacitors in the actual modeling. The impedance of a CPE (Z_{CPE}) is described by the equation

$$Z_{CPE} = \frac{1}{C(j\omega)^P} \quad (1)$$

where C is the capacitance of an element that would be found if $P = 1$, j is the square root of -1, ω is the frequency and P is a unitless coefficient loosely related to the distribution of the relaxation times, with $P = 1$ corresponding to a single relaxation time.

TABLE 1: Fitted Parameters

	$HLaNb_2O_7 \cdot 0.5H_2O$	$HLaTa_2O_7 \cdot xH_2O$
R_{ionic}	263 kΩ·cm	41 kΩ·cm
C_{geom}	160 nF/cm^2	524 pF/cm^2
p_{geom}	0.56	0.92
R_{ct}	13 MΩ·cm	630 kΩ·cm
C_{dl}	55 μF/cm^2	70 μF/cm^2
p_{dl}	0.74	0.51

Although an (RC)-(RC)-type arrangement shown in Figure 2a is perhaps more commonly encountered in the literature, we note that given the same R and CPE values, the circuit shown in Figure 2b gives exactly the same spectra as that in Figure 2a does in both Nyquist and Bode plots. Other than the presence of R_{ct}, This second circuit is the same as the one used by Thangadurai et al. to model electrolytes with blocking electrodes,[21] and provides a basis for the circuit shown in Figure 5b. For fitting, a least-squares optimization was initially conducted using the first model circuit, and it was confirmed that the second model circuit in Figure 2b gave the same impedance spectra. The results are summarized in Table 1.

For these types of materials, C_{geom} and C_{dl} have been reported to be typically in the range of a few pF/cm^2 and μF/cm^2, respectively.[21] Although the tantalate compound gives values of similar magnitude, it is not clear why C_{geom} for the niobate is different. For other spectra reported here, it was difficult to fit R_{ct} with high accuracy, often because the curvature of the semicircle was not very pronounced. The varying values of R_{ct} are thought to be a reflection of the varying pseudo-blocking character of the Pt electrodes.

$HLaNb_2O_7$ is known to be reduced reversibly by H_2, even at ambient temperature.[22,23] The equilibrium corresponding to a complete reduction can be expressed as follows:

$$H_2 + HLaNb_2O_7 \leftrightarrow HLaNb_2O_6 + H_2O$$

In terms of developing useful ionic conductors, this reaction is problematic, since the original compound is a Nb(V) compound and reduction gives a mixture of +V and +IV oxidation states, leading to electronic conduction. Focusing on the water byproduct of the forward reaction, the redox equilibrium can be pushed backward with the addition of water vapor to the hydrogen stream. An experiment was run in which a small amount of $HLaNb_2O_7$ was heated in dry and wet hydrogen. In dry hydrogen, the material turned dark blue; this color change can be attributed to an intervalence charge-transfer band centered at 1100 nm,[22] which indicates that the material has been reduced. However, the blue color does not appear when 0.3 atm of water vapor is added to the hydrogen stream, indicating that reduction has been suppressed substantially. Figure 3b shows electronic conductivity measurements of a $HLaNb_2O_7$ pellet, where the DC, or electronic conductivity has been lowered by an order of magnitude by the introduction of water. In Figure 3a, the sample was treated at the indicated temperature, and then as the temperature was ramped down, the DC conductivity was measured. The figure shows that the activation energy for conduction remains fairly constant, regardless of the treatment, but it is the change in intercept, or density of charge carriers, that lowers the conductivity. This is consistent with the equilibrium shift mechanism mentioned earlier, as the introduction of water vapor changes only the position of the equilibrium,

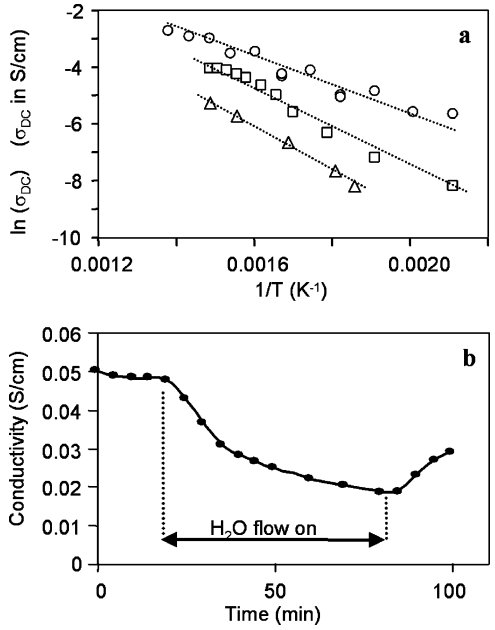

Figure 3. (a) Effects of H_2 pretreatment on σ_{DC} of $HLaNb_2O_7 \cdot 0.5H_2O$ ($P_{H_2O} = 0.3$ atm). ○: 450 °C dry H_2, □: 400 °C dry H_2, △: 400 °C wet H_2. (b) Effect of water on DC conductivity under H_2 at 400 °C, $P_{H_2O} = 0.3$ atm.

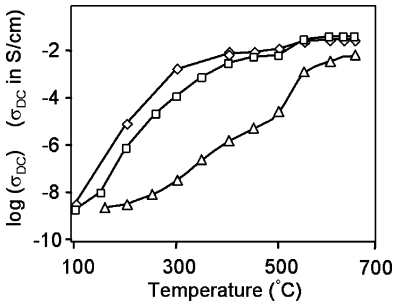

Figure 4. DC conductivity of $HLaABO_7$ (A, B = Nb, Ta) in dry H_2. ◇: $HLaNb_2O_7$, □: $HLaNbTaO_7$, △: $HLaTa_2O_7$.

and not the mechanism for electronic conduction. The sample treated under dry hydrogen at 450 °C is an *n*-type semiconductor with an activation energy for conduction of 0.77 eV. As Palacin et al. found,[23] plotting $-\ln(\sigma)$ vs $1/(T^{1/4})$ failed to give any significantly better fits to the data, so it is not clear whether a variable range hopping mechanism is operative or not.[24]

Because the niobium cation is easier to reduce to lower, stable oxidation states (as in NbO, NbO_2, etc.) than is the tantalum cation, the analogous Dion−Jacobson phase was synthesized with tantalum as the B-site cation, in order to suppress electronic conductivity. Figure 4 shows that the electronic conductivity is suppressed by several orders of magnitude, particularly at intermediate temperatures.

Effect of Hydrogen and Elevated Temperature on Impedance. Since these materials were studied as potential candidates for intermediate temperature fuel cell membranes, it is important to know how stable they are at elevated temperatures and under reducing conditions. Figure 5**a** shows impedance spectra for $HLaNb_2O_7 \cdot 0.5H_2O$ and $HLaTa_2O_7 \cdot xH_2O$ in contact with humidified H_2 and air. Here, the niobate compound loses its low-frequency tail when the atmosphere is switched to wet hydrogen, but the same effect is not seen for the tantalate. The model in Figure 5b explains the difference in the impedance behavior. Under wet air, there is very little electronic conductivity in either material, so the equivalent circuit previously shown in Figure 2 is adequate to model the spectra. Under wet hydrogen,

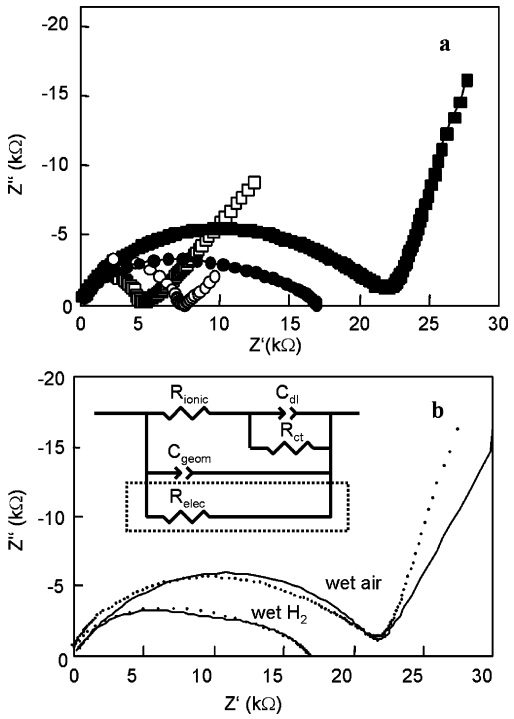

Figure 5. (a) Impedance spectra of $HLaNb_2O_7 \cdot 0.5H_2O$ and $HLaTa_2O_7 \cdot xH_2O$ at room temperature under humidified air and H_2 ($P_{H_2O} = 0.03$ atm). Frequencies range 1 MHz ∼ 0.1 Hz. □: $HLaTa_2O_7 \cdot H_2O$, wet air, 5.5 h; ■: $HLaNb_2O_7 \cdot 0.5H_2O$, wet air, 5.5 h; ○: $HLaTa_2O_7 \cdot xH_2O$, wet H_2, 1 h; ● $HLaNb_2O_7 \cdot 0.5H_2O$, wet H_2, 1 h. (b) Spectra for $HLaNb_2O_7 \cdot 0.5H_2O$ in different atmospheres, reproduced from (a). Modeled results are shown by solid lines, and R_{elec} was added for the wet H_2 sample.

however, the equivalent circuit is shorted by an electronically conducting pathway, shown by R_{elec} in Figure 5b. This results in a lack of tail at low frequencies, which explains why the shape is changed when wet hydrogen is applied. Ideally, the circuit in Figure 5b should show two semicircles; a low-frequency relaxation with its real intercept at R_{elec} and another one at higher frequency with an intercept equal to $(R_{elec}^{-1} + R_{ionic}^{-1})^{-1}$. We do not see this probably because the RC components are not separated enough from each other and the semicircles are depressed. While this makes it difficult to obtain an unambiguous fit, the solid lines shown in Figure 5b show that it is possible to model the spectra of the niobate in wet H_2 by simply adding an R_{elec} component (108 kΩ·cm) while keeping R_{ionic} the same as before reduction (140 kΩ·cm). The reasons for the conductivity in the tantalate *decreasing* slightly when exposed to wet hydrogen (Figure 5a) are not known. In general, the results from Figure 5 indicate that, even at room temperature under humidified conditions, $HLaNb_2O_7 \cdot 0.5H_2O$ is reduced to form a mixed ionic-electronic conductor.

Higher temperature measurements on $HLaNb_2O_7$ under humidified H_2 are shown in Figure 6. At 110 °C, a flattened semicircle is observed, similar to that seen in Figure 5. This feature gradually changes into a single semicircle as the temperature is increased. As the temperature is increased, the niobate is progressively reduced, which, in terms of Figure 5b, implies a decreasing R_{elec}, resulting in the lower frequency semicircle becoming smaller. The end result is a single semicircle obtained at 400 °C (Figure 6). Here, the material is reduced to a predominantly electronic semiconductor, which is modeled by a parallel $R_{elec}C_{geom}$ circuit, showing a single semicircle with no tail. Upon cooling in the humidified H_2 stream, the material remains an electronic semiconductor, and

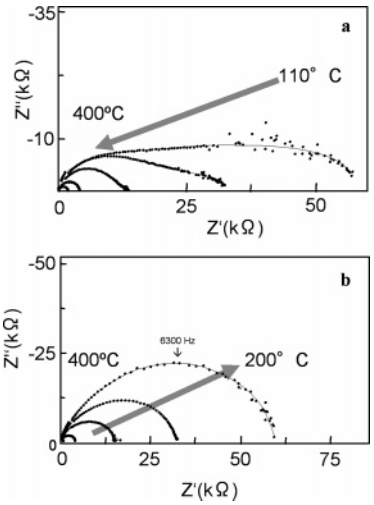

Figure 6. Impedance spectra of $HLaNb_2O_7$ at elevated temperatures in humidified hydrogen (P_{H_2O} = 0.3 atm) upon heating (a) and cooling (b).

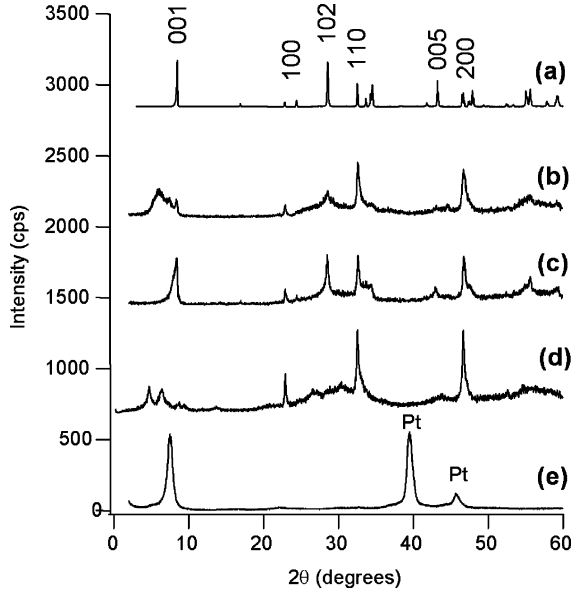

Figure 7. X-ray diffraction patterns of $HLaNb_2O_7$ with a modified layer structure: (a) parent $HLaNb_2O_7$, (b) restacked, (c) heat treated, (d) silica-pillared, and (e) cast $HLaNb_2O_7$ film on Pt/glass.

thus the shape remains constant. The semicircle increases in size, however, since the material is a semiconductor and electronic conductivity decreases as the temperature decreases.

Characterization of Pillared Samples. Trace a in Figure 7 is the X-ray diffraction pattern of the parent material $HLaNb_2O_7$. The reflection at 8.4° indicates an interlayer (00l) spacing of 10.4 Å. Stepwise intercalation of hexylamine, decylamine, and the organosiloxane modifies the layer to 24.2, 29.4, and ~23.4 Å, respectively. The organosiloxane seems to intercalate better when dissolved in ethanol rather than when treated as a sol in water. However, calcining the former sample led to a smaller interlayer spacing and smaller surface area.

Thermal gravimetry coupled with mass spectrometry showed that both materials can be calcined at 450−500 °C to remove all organic traces. X-ray diffraction shows, however, that calcination at higher temperatures collapses the pillars. BET surface area measurements for both samples gave surface areas of 13.5 m^2/g for the water sol sample and 9.1 m^2/g for the ethanol solvent sample, whereas the original unpillared $HLaNb_2O_7$ has a surface area of less than 1 m^2/g. Scanning electron microscopy images of the pillared material are shown in Figures 8. EDS showed abundant silicon. The surfaces of the particles appear to be relatively smooth, however, and this implies that the high surface area is due to silica pillaring rather than a porous layer of silica forming on the external surface of the lanthanum niobate particles.

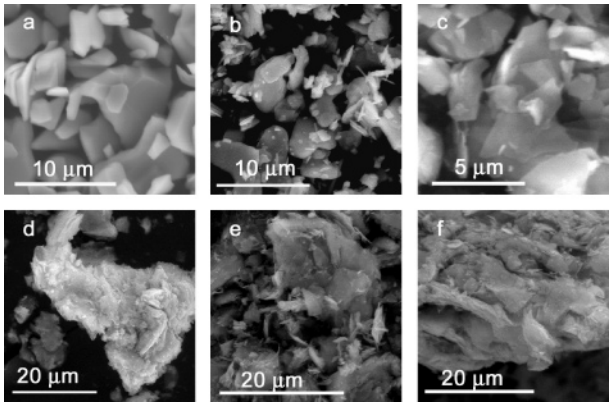

Figure 8. Scanning electron microscopy images of (a) parent $HLaNb_2O_7$, (b) $HLaTa_2O_7$, (c) silica-pillared $HLaNb_2O_7$, (d) restacked/UV-O_3 treated $HLaNb_2O_7$, (e,f) further heat treated d.

Characterization of Flocculated Samples. $HLaNb_2O_7$ was exfoliated into nanometer-thick and micron-wide sheets by stirring in excess aqueous TBAOH. When flocculated by addition of acid, the sheets re-assemble in a disordered manner, as can be see in the X-ray diffraction comparison in Figure 7b. The broadened and shifted 00l line indicates that the layered structure has been severely altered, with most layers further apart from each other than in the parent compound. The loss of intensity in the three-dimensional reflections, such as 102, in comparison with the 110 line, implies that the layers are disoriented with respect to each other, and the asymmetric profile of the 110 line also implies that the orientation between layers has been lost.[25] Nitrogen adsorption−desorption isotherms shown in Figure 9 exhibit large hysterisis for only the flocculated compound, implying the existence of mesopores. The BET surface area for this compound is 29 m^2/g, which is even larger than that of the pillared samples. The material was treated with UV−O_3, but it is possible that some residual organics remain.

When the flocculated material was annealed in air at 350 °C overnight, the high surface area was retained (35 m^2/g). The mesopores have disappeared, however, as the isotherm in Figure 9b does not show adsorption−desorption hysterisis. The X-ray diffraction pattern shown in Figure 7c shows that much of the original layered structure was recovered, but with a noticeably smaller crystallite size. The slight increase in surface area upon annealing may be due to residual organic material being removed during heating.

Effect of Structure on Impedance Measurements. In general, the room-temperature impedance response for the parent material, the pillared, and annealed materials are largely similar (Figure 10a). At high frequencies, an experimental artifact where the impedance jumps into the second quadrant is seen; this is most likely due to phase shift in the operational amplifiers of the potentiostat. It is surprising that, although the pillared and annealed materials differ greatly in surface area and hence water adsorption capacity, the conductivity does not change significantly. The exception in Figure 10a is the response of the restacked but non-annealed $HLaNb_2O_7$ (inverted open triangles), which shows that the inside circle is much smaller than in the

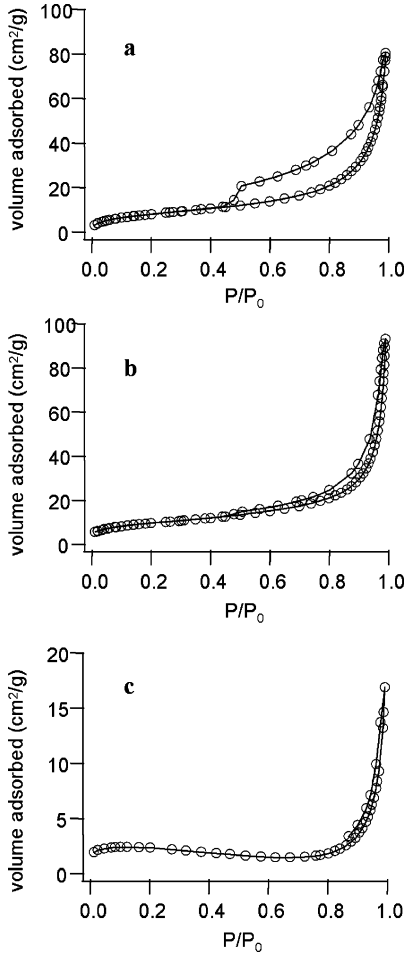

Figure 9. Nitrogen adsorption isotherms at 77 K of (a) flocculated $HLaNb_2O_7$, (b) $HLaNb_2O_7$ flocculated and then annealed at 350 °C, and (c) silica -pillared $HLaNb_2O_7$.

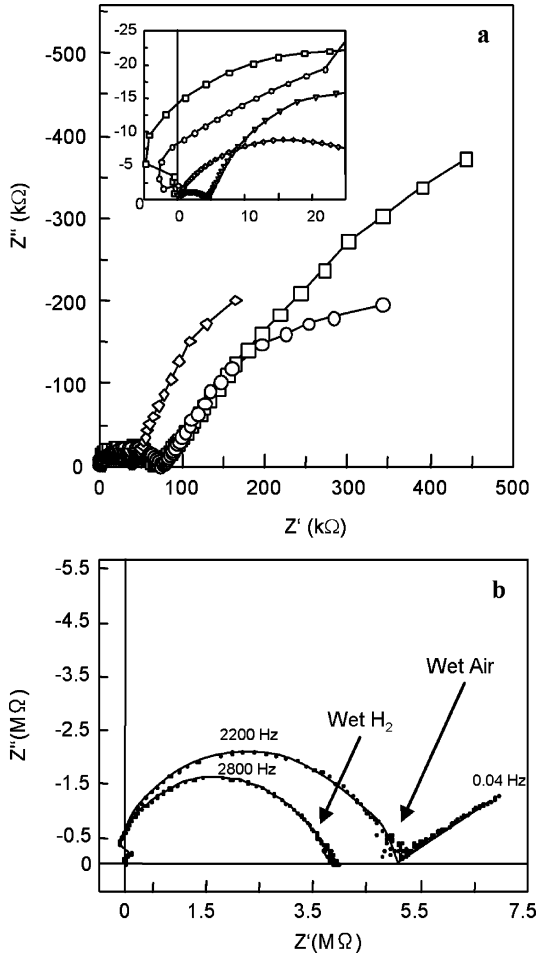

Figure 10. Impedance spectra for various modified $HLaNb_2O_7 \cdot 0.5H_2O$ samples at room temperature, 100% RH air equilibrated overnight. Lower limit of frequency is 0.01 Hz unless otherwise noted. (a) Various pelletized samples: ◇: original $HLaNb_2O_7 \cdot 0.5H_2O$, □: SiO_2-pillared, ▽: restacked ○: restacked, annealed. (b) Comparison of oriented film under different atmospheres (equilibrated 1.5 h).

other samples. The moderately large surface area created by pillaring (9 m^2/g) does not have such a large effect on conductivity. Although the restacked material has an even larger surface area (29 m^2/g), the gain in conductivity obtained here is disproportionately large considering that increased surface area had no affect for the pillared sample.

Furthermore, this enhanced conductivity of the restacked sample is lost when it is annealed to recover a regular layered structure. We assume that the annealed material has not been irreversibly dehydrated to $LaNb_2O_{6.5}$ during thermal annealing at 350 °C, since the position of the 001 line of the annealed material coincides with that of the parent $HLaNb_2O_7$. Instead, the difference in conductivity of the restacked material from others is perhaps due to structural differences illustrated schematically in Figure 11.

In all cases, we expect conduction to be due to grain surface conduction. We use the term grain *surface* as opposed to grain *boundary* because our sample pellets are not sintered and contain many voids. In the restacked material, the structure reflects the flexible nature of the exfoliated sheets—the individual sheets mesh well so that contact with each sheet occurs over a wide area, and there are many points of contact as sketched in Figure 11a. Therefore, the loss in conductivity due to sheet-to-sheet transfer is low. Once the material is annealed, however, X-ray diffraction shows the recovery of well ordered layers. This is only possible if a granular structure with distinct grains and voids is recovered. Now, contact between each grain is more limited, and the overall conductivity is decreased. Although the grain−grain contact points are in series with the grain surface conduction pathways, we cannot distinguish them as independent relaxations in the impedance spectra.

An alternative explanation is that somehow the presence of mesopores as opposed to other pore diameters is crucial to the hydration of the surface and its effect on proton conductivity. The pillared sample, possessing very narrow pores, and the annealed sample whose surface area comes from inter-grain voids and simply thinner crystallites, did not show enhanced conductivity despite having a relatively high surface area.

Effect of Orientation. Ethanol suspensions of exfoliated $HLaNb_2O_7$ were deposited to form thin films on Pt contacts with a glass support. As the X-ray diffraction pattern in Figure 7 suggests, the layers are predominantly oriented parallel to the substrate plane. Immediately after deposition the interlayer distance has been expanded (d = 18.6 Å) due to intercalation of tetrabutylammonium hydroxide and perhaps residual solvent, but most of this can be removed by either UV−O_3 treatment or by thermal treatment at 350 °C.

In-plane measurements for the oriented film (70 nm thick, 17 mm wide, and across a gap 800 μm wide) yielded the impedance spectra shown in Figure 10b. As in the pellet case shown in Figure 4a, when treated with hydrogen, the material becomes more conductive and shows no tail at low frequency, indicating that it is electronically conducting. For the film sample, the semicircle is less depressed since the grains are more

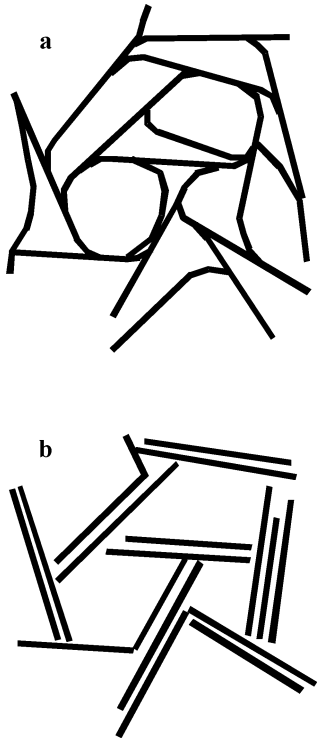

Figure 11. Schematics of structure in (a) restacked $HLaNb_2O_7 \cdot 0.5H_2O$ and (b) subsequent annealing at 350 °C

aligned among themselves and with the Pt electrodes. This gives a well-defined RC time constant, which results in a less depressed semicircle.

The resistance of the film at the intercept on the real axis of Figure 10b corresponds to a resistivity of 730 Ω·cm, whereas the pelletized samples typically are around 140−600 kΩ·cm. Thus, the oriented film is nearly 3 orders of magnitude more conductive than are the pellets with randomly oriented grains. This is expected given the high aspect ratio of the sheets, and similar cases have been reported previously with oriented pellicular films of zirconium phosphate.[7,26]

Conclusions

Although $HLaNb_2O_7 \cdot 0.5H_2O$ readily reduces under hydrogen to give significant electronic conduction, its ionic conductivity can be increased significantly by exfoliation/flocculation to modify surface conduction pathways. This structure might be stabilized with inorganic pillars, so that it does not collapse at higher temperatures. Conduction pathways can also be optimized by preparing thin, oriented films. The electronic conductivity can be suppressed by the addition of water vapor and by substituting the B-site cation with a less reducible element, such as tantalum.

Acknowledgment. This work was supported by the National Science Foundation under Grant CHE-0095394. We also thank an anonymous reviewer for valuable comments on interpreting the impedance spectra, the Winograd group for use of their profilometer, and Adrian Goodey for obtaining the SEM images.

Supporting Information Available: XRD patterns of $HLaNb_2O_7$ and B-site analogues; TGA plots of $HLaNb_2O_7$ and $HLaTa_2O_7$; images of $HLaNb_2O_7$ under wet hydrogen and air at elevated temperature; Kramers−Kronig transforms of select impedance data. This material is available free of charge via the Internet at http://pubs.acs.org.

References and Notes

(1) Norby, T. *Solid State Ionics* **1999**, *125*, 1.
(2) Li, Q.; He, R.; Jensen, J. O.; Bjerrum, N. J. *Chem. Mater.* **2003**, *15*, 4896.
(3) Asensio, P. G. e.-R. *Fuel Cells* **2005**, *5*, 336.
(4) Iwahara, H.; Uchida, H.; Ono, K.; Ogaki, K. *J. Electrochem. Soc.* **1988**, *135*, 529.
(5) (a) Du, Y.; Nowick, A. S. *Solid State Ionics* **1996**, *91*, 85.
(6) Liang, K. C.; Du, Y.; Nowick, A. S. *Solid State Ionics* **1994**, *69*, 117.
(7) Boysen, D. A.; Uda, T.; Chisholm, C. R. I.; Haile, S. M. *Science* **2004**, *303*, 68.
(8) Alberti, G.; Casciola, M.; Costantino, U.; Leonardi, M. *Solid State Ionics* **1984**, *14*, 289.
(9) Guo, C.-x.; Hou, W.-h.; Guo, M.; Yan, Q.-j.; Chen, Y. *Chem. Commun.* **1997**, 801.
(10) Matsuda, T.; Udagawa, M.; Kunou, I. *J. Catal.* **1997**, *168*, 26.
(11) Schaak, R. E.; Mallouk, T. E. *Chem. Mater.* **2000**, *12*, 2513.
(12) Schaak, R. E.; Mallouk, T. E. *Chem. Mater.* **2002**, *14*, 1455.
(13) Matsuda, T.; Fujita, T.; Miyamae, N.; Takeuchi, M.; Kanda, K. *Bull. Chem. Soc. Jpn.* **1993**, *66*, 1548.
(14) Sato, M.; Abo, J.; Jin, T.; Ohta, M. *J. Alloys Compd.* **1993**, *192*, 81.
(15) Thangadurai, V.; Shukla, A. K.; Gopalakrishnan, J. *Solid State Ionics* **1994**, *73*, 9.
(16) Thangadurai, V.; Weppner, W. *Solid State Ionics* **2004**, *174*, 175.
(17) Sato, M.; Jin, T.; Uematsu, K. *J. Solid State Chem.* **1993**, *102*, 557.
(18) Macdonald, D. D.; Sikora, E.; Engelhardt, G. *Electrochim. Acta* **1998**, *43*, 87.
(19) Gopalakrishnan, J.; Bhat, V. *Mater. Res. Bull.* **1987**, *22*, 413.
(20) Norby, T.; Widerøe, M.; Glöckner, R.; Larring, Y. *Dalton Trans.* **2004**, 3012.
(21) Thangadurai, V.; Huggins, R. A.; Weppner, W. *Electrochem. Soc. Proc.* **2001**, *109*, 2001−28.
(22) Gomez-Romero, P.; Palacin, M. R.; Casan, N.; Fuertes, A. *Solid State Ionics* **1993**, *424*, 63−65.
(23) Palacin, M. R.; Lira, M.; Garcia, J. L.; Caldes, M. T.; Casan-Pastor, N.; Fuertes, A.; Gomez-Romero, P. *Mater. Res. Bull.* **1996**, *31*, 217.
(24) Mott, N. *Conduction in Non-Crystalline Materials*; Oxford University Press: Oxford, 1987.
(25) Warren, B. E. *Phys. Rev.* **1941**, *59*, 693.
(26) Alberti, G.; Casciola, M.; Massinelli, L.; Palombari, R. *Ionics* **1996**, *2*, 179.